Thermal and Morphological Characterization of Nanocomposites Prepared by in-Situ Polymerization of High-Density Polyethylene on Carbon Nanotubes

M. Trujillo, M. L. Arnal, and A. J. Müller*

Departamento de Ciencia de los Materiales, Universidad Simón Bolívar, Apartado 89000, Caracas 1080-A, Venezuela

E. Laredo

Departamento de Física, Universidad Simón Bolívar, Apartado 89000, Caracas 1080-A, Venezuela

St. Bredeau, D. Bonduel, and Ph. Dubois

Center of Research and Innovation in Materials & Polymers CIRMAP, Service des Materiaux Polymeres et Composites SMPC, Université de Mons-Hainaut, Place du Parc 20, B-7000 Mons, Belgium

Received May 5, 2007; Revised Manuscript Received June 21, 2007

ABSTRACT: The morphology, nucleation, and crystallization of polyethylene/carbon nanotubes nanocomposites were studied. The nanocomposites were prepared by in-situ polymerization of ethylene on carbon nanotubes (CNT) whose surface had been previously treated with a metallocene catalytic system. The effects of composition (5−22% CNT) and structure of the nanotube (single, double, or multiwall, i.e., SWNT, DWNT, and MWNT) were evaluated, and an excellent nucleating effect on polyethylene matrix was found regardless of the CNT type in comparison to neat high-density polyethylene (HDPE) prepared under identical conditions. The CNT were found to be more efficient in nucleating the HDPE than its own crystal fragments, a result obtained by self-nucleation studies. Differential scanning calorimetry (DSC) and transmission electron microscopy (TEM) results showed that under both isothermal and dynamic crystallization conditions the crystals produced within the nanocomposite HDPE matrix were more stable than those produced in neat HDPE or in physical blends prepared by melt mixing of HDPE and untreated CNT. The remarkable stability of the crystals was reflected in melting points up to 5 °C higher than neat HDPE and concomitant thicker lamellae. The changes induced on HDPE by CNT are due to the way the nanocomposites were prepared; since the macromolecular chains grow from the surface of the nanotube where the metallocene catalyst has been deposited, this produces a remarkable nucleating effect and bottle brush morphology around the CNT. Isothermal crystallization kinetics results showed that the in-situ nanocomposites crystallize much faster at equivalent supercoolings than neat HDPE because of the nucleating effect of CNT. Wide-angle X-ray scattering studies demonstrated that the crystalline structure of the HDPE matrix within the in-situ-polymerized HDPE/CNT nanocomposites was identical to that of neat HDPE and did not change during isothermal crystallization, keeping its orthorhombic unit cell.

1. Introduction

Since their introduction in 1991, carbon nanotubes (CNT) have attracted much attention.[1] Their high flexibility, low mass density, and high aspect ratio (300−1000), in addition to their excellent mechanical, thermal, and electrical properties, have turned them into potential candidates to create multifunctional polymeric nanocomposites.[2−4] From the preparation of the first polymeric nanocomposite incorporating CNT by Ajayan et al. in 1994,[5] several researchers have explored the potentiality of such nanocomposites. This has been reflected in the growing number of patents and publications to date.[6]

One of the problems with the preparation of polymeric nanocomposites with CNT is the difficulty of dispersing them. Their small size, large superficial area, and the presence of π electrons highly delocalized in their surfaces make them susceptible to van der Waals forces that promote aggregation.[2,3] Many techniques have been applied to attempt the dispersion of CNT in polymeric matrices, for example, the application of ultrasound and chemical modification of the CNT surface.[3,6−9]

Another method involves the dispersion in solvents of the CNT with surfactants and high-frequency ultrasound. In this way, suspensions are achieved in which a polymer is later dissolved, and the nanocomposite is prepared by solvent evaporation. Both water-soluble polymers and polymers soluble in organic solvents have been employed.[6,10−16] Although, using this method, nanocomposites with substantial modification of mechanical and dielectric properties of the polymeric matrix have been achieved, it is impractical for large-scale applications.[17−19]

Dubois et al.[20] have recently introduced a novel way to avoid aggregation. The method is derived from the polymerization-filling technique (PFT) initially employed in Ziegler−Natta polymerization studies[21,22] and more recently developed for the application of metallocene-based catalysts to a wide range of microfillers, such as kaolin, silica, wollastonite, graphite, and glass microspheres.[23−26] The method consists of in-situ polymerization of ethylene catalyzed by a highly active metallocene-based catalytic complex that has a peculiar feature—it is physicochemically grafted to the CNT surface. As a result, individual CNT are homogeneously coated by polyethylene

* Corresponding author.

10.1021/ma071025m CCC: $37.00
Published on Web 07/27/2007

chains that grow on their surfaces, causing deaggregation of the CNT. The material thus formed can be used directly or as a masterbatch for future preparations of nanocomposites with polymeric matrices in the melt, depending on the concentration of CNT. The present work aims at reporting the effect of the content and type of CNT on the morphology and thermal behavior of different HDPE/CNT nanocomposites prepared by the in-situ polymerization of ethylene on CNT whose surfaces were previously impregnated by the catalytic system, as described elsewhere.[20]

Several previous works have studied the changes in morphology and nucleation that can be induced in a polymeric semicrystalline matrix by the incorporation of CNT.[27−32] Bhattacharyya et al.[27] have shown that single-wall carbon nanotubes (SWNT) are capable of nucleating isotactic polypropylene, PP, with just 0.8% by weight, thereby reducing spherulitic size as expected. Grady et al.[28] and Aussoline et al.[29] found nucleating effects of carbon nanotubes on PP during isothermal and nonisothermal kinetics experiments. A nucleation effect of SWNT has also been observed for poly(vinyl alcohol), PVA.[30,31] Also, Minus et al.[31] and Haggenmueller et al.[32] found that SWNT not only acted as a nucleating agent for poly(vinyl alcohol) and PE, respectively, but also templated the morphology of the polymers, since their growth direction was always perpendicular to the CNT.

2. Experimental Section

2.1. Sample Preparation. HDPE/CNT nanocomposites were obtained by a soft method derived from the polymerization-filling technique (PFT) using metallocene catalysis.[20] PFT applied to carbon nanotubes consists in anchoring methylaluminoxane (MAO), a well-known cocatalyst used in metallocene-based olefin polymerization process, onto the surface of carbon nanotubes in suspension in dried heptane. A metallocene catalyst, Cp_2*ZrCl_2 in this study (where Cp stands for cyclopentadienyl), is then reacted with the surface-activated carbon nanotubes. Addition of ethylene leads to the synthesis of polyethylene (HDPE) exclusively at the surface of the carbon nanotubes. Such a coating limits the formation of airborne carbon nanotubes aggregates, making handling much safer.

Materials. All air- and moisture-sensitive compounds (e.g., catalyst and cocatalyst) were manipulated using standard vacuum line, Schlenk, or cannula techniques under dry nitrogen or in a glovebox under a deoxygenated and dry nitrogen atmosphere (O_2 and H_2O < 1 ppm). *n*-Heptane was dried and stored over molecular sieves (4 Å) while toluene was refluxed over CaH_2 and freshly distilled prior to use under a N_2 atmosphere. Bis(pentamethyl-η^5-cyclopentadienyl)zirconium(IV) dichloride ($Cp*_2ZrCl_2$) was purchased from Aldrich, used without further purification, and then stored at 4 °C as a stock solution in toluene with a known concentration (5.2 mM). MAO (30 wt % solution in toluene) was kindly supplied by Total Petrochemicals Research Feluy (Belgium) and diluted in dried toluene with a known concentration (1.31 M). Ethylene (Air Liquide, 99.95%) was used without further purification. All carbon nanotubes were kindly supplied by Nanocyl S.A. and were previously dried at 105 °C under reduced pressure (10^{-2} mmHg) for 8 h and then stored under a N_2 atmosphere. The polymerization reactions were performed in a glass reactor by following the ethylene consumption with a Zipperclave batch reactant gas delivery system (BRGDS).

Representative Procedure for Polymerization. *(i) Carbon Nanotube Surface Activation.* A 250 mL polymerization flask was filled with 0.25 g of MWNTs and flame-dried under high vacuum. The flask was then filled with nitrogen and placed in an oil bath at 50 °C. 20 mL of dried and deoxygenated *n*-heptane and 1.10 mL of MAO (1.31 M) were added under nitrogen. The CNTs in contact with the aluminoxane were stirred for 1 h at 50 °C. Solvents were then distilled off at 50 °C under reduced pressure. The solvents, together with any volatile organoaluminum compounds, were trapped in a flask cooled by liquid nitrogen for aluminum titration. Treated CNTs were further heated up at 150 °C under reduced pressure for 90 min.

Table 1. Compositions of the HDPE/CNT Samples Evaluated: HDPE/SWNT ($PE_xS_yA_z$), HDPE/DWNT ($PE_xD_yA_z$), and HDPE/MWNT ($PE_xM_yA_z$)

composition	type	CNT content (%)	HDPE content (%)	Al_2O_3 content (%)
HDPE			92.4	7.6
$PE_{87}S_8A_5$	SWNT	7.6	87.1	5.4
$PE_{56}S_{20}A_{24}$	SWNT	20.1	56.1	23.9
$PE_{33}S_{36}A_{31}$	SWNT	33.2	36.2	30.6
$PE_{82}D_8A_{10}$	DWNT	7.6	82.2	10.2
$PE_{60}D_{17}A_{23}$	DWNT	17.4	60.2	22.5
$PE_{44}D_{26}A_{30}$	DWNT	26.2	43.5	30.4
$PE_{83}M_6A_{11}$	MWNT	5.9	82.6	11.5
$PE_{68}M_{11}A_{21}$	MWNT	11.2	68.2	20.6
$PE_{41}M_{26}A_{33}$	MWNT	26.4	41.1	32.5

(ii) Polymerization Step. The polymerization reactions were performed in a 250 mL glass reactor by following the ethylene consumption with a BRGDS device. The aluminoxane-treated CNTs were dispersed in 20 mL of dried *n*-heptane. Then, 0.80 mL of $Cp*_2ZrCl_2$ (4.1 μmol in Zr, [Al]/[Zr] = 350) was added to the suspension. The stirred mixture was then heated up to 50 °C for 15 min. The reactor was purged by ethylene (0.5 min) in order to remove nitrogen. The polymerization reaction was carried out under a constant pressure of 13 bar of ethylene at 50 °C and vigorous stirring for a defined period of time. The final material was precipitated in 200 mL of methanol acidified with hydrochloric acid and filtered off. This step allowed for both recovering the HDPE-coated nanotubes and deactivating the catalytic complex yielding residual aluminum oxide (Al_2O_3) in all samples. The resulting material was then dried at 60 °C for ca. 12 h in a ventilated oven.

Table 1 shows the composition and identification of all the samples employed in this work. For comparison purposes, a neat HDPE homopolymer was synthesized employing similar conditions to those used for the nanocomposites. Three types of CNT were employed: single wall (SWNT), double wall (DWNT), and multiwall (MWNT). The compositions of the samples are given by the following nomenclature: $PE_xS_yA_z$, where the subscripts indicate the weight contents in percent of each component present in the formulation (HDPE, CNT, and Al_2O_3, respectively); the letter S is used to denote the use of SWNT, and other samples with letters D or M indicate DWNT or MWNT. The compositions were determined by thermogravimetry analysis (TGA).

Table 1 also shows that the CNT are present in the samples in three different contents: low (5−8%), medium (11−20%), and high (26−33%). The highest contents of CNT are present in SWNT systems. The CNT employed had different diameters: 2, 4, and 5−27 nm for SWNT, DWNT, and MWNT, respectively. These diameters were determined by transmission electron microscopy (TEM) (see Figure 1).

2.2. Morphological Evaluation (TEM). The morphological observations were performed by TEM, with a JEOL instrument, model JEM 1220, at 100 kV operation voltage. Lamellar thicknesses measurements were performed on micrographs taken after samples were isothermally crystallized for 7 days at 124 °C. They were later embedded in resin and cut with a diamond knife in a Leica ultracryomicrotome. The thin sections thus obtained were stained with RuO_4 vapors.

2.3. Thermal Characterization. Calorimetric studies were carried out in a Perkin-Elmer Pyris 1 differential scanning calorimeter (DSC) calibrated with indium and tin. Ultrahigh-purity nitrogen was used as a purge gas. Samples of ∼5 mg each were encapsulated in aluminum pans and sealed. The crystalline thermal history was erased by heating the samples at 170 °C for 3 min.[33] Cooling and subsequent heating scans were registered at 10 °C/min.

Self-Nucleation Tests (SN). In order to evaluate the nucleation capacity of CNT on HDPE, self-nucleation tests (SN) were performed according to procedures devised originally by Fillon et

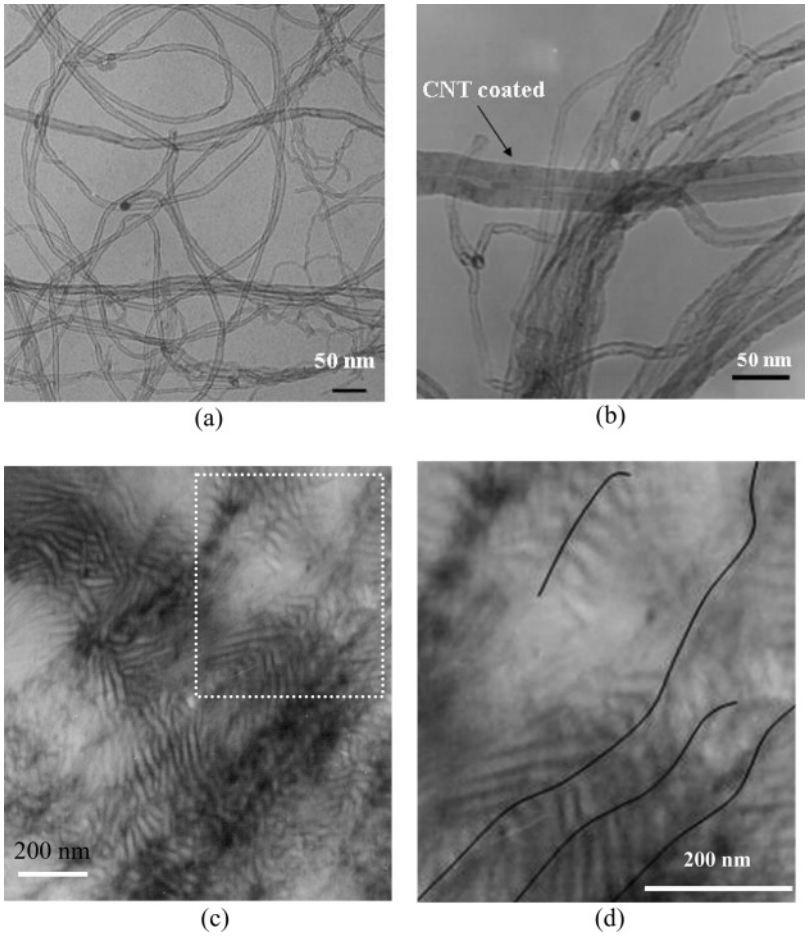

Figure 1. TEM micrographs of (a) MWNT, (b) $PE_{41}M_{26}A_{33}$ sample (as obtained from polymerization reactor), and (c) $PE_{83}M_6A_{11}$ after isothermal crystallization for 1 week at 124 °C and (d) details of region indicated in (c) with a white square.

al.[33−35] The complete thermal treatment comprises the following: (a) Erasure of crystalline thermal history by heating the sample to 170 °C for 3 min. (b) Creation of a "standard" thermal history by cooling at 10 °C/min to 25 °C. (c) Partial melting up to a temperature denoted T_s, depending on which the sample will be completely molten, just self-nucleated, or self-nucleated and annealed. If T_s is too high, the molten sample is said to be in "domain I" or complete melting domain. If T_s is high enough to melt the sample almost completely but low enough to induce self-nucleation without annealing, the sample is said to be under "domain II" or self-nucleation domain (for details on the nature of domain II, see ref 35). If T_s is low enough, only part of the crystal population will be molten, and therefore the unmelted crystals will experience annealing during the 3 min at T_s (step d). Upon subsequent cooling, the molten polymer will crystallize self-nucleated by the annealed crystal fragments that were not melted. Then the sample is said to be in domain III or self-nucleation and annealing domain. (d) Thermal conditioning at T_s during 5 min. (e) DSC cooling scan from T_s, where the effects of the thermal treatment will be reflected on the crystallization of the HDPE.

Isothermal Crystallization Kinetics. The samples were first heated to 170 °C in order to erase all crystalline thermal history and kept in the melt for 3 min before they were quenched (by controlled cooling in the DSC at 60 °C/min) to the chosen isothermal crystallization temperature, T_c. In order to choose the crystallization temperature range, preliminary tests were run by quenching the sample to a specific T_c and then immediately heating it while recording its heating scan in DSC at 10 °C/min. If any melting was observed, it indicated that the sample was able to crystallize during the quenching at 60 °C/min. Therefore, this crystallization temperature was not employed, and the same test was performed at higher temperatures until no crystallization during the quenching was obtained. This procedure was used to find the lowest T_c, and then isothermal crystallization experiments were run every half a degree from that T_c upward in temperature until the crystallization exotherm was too small to be detected by the DSC. This procedure is the usual to obtain continuous isothermal crystallization (CIC) data with the DSC.

2.4. Wide-Angle X-ray Diffraction (WAXS). WAXS experiments were carried on as-prepared neat PE and nanocomposite samples in an X'Pert automatic diffractometer using Ni-filtered Cu Kα radiation. The spectra were recorded in an angular range $10° \leq 2\theta \leq 46°$ at room temperature by counting for 10 s every 0.01° step. The effect on the crystal structure and on the sample crystallinity of the addition of different types of CNT in various concentrations was thus followed.

3. Results and Discussion

3.1. Morphological Evaluation. A TEM morphological evaluation of neat nanotubes and of the prepared nanocomposites was performed. In the case of neat CNT, a dispersion in water/alcohol mixture was made with an ultrasound sonicator. Droplets of these suspensions were placed on electron microscopy gold grids and dried before their observation by TEM. Figure 1a shows a representative micrograph of MWNT; from micrographs such as these, the average diameters of the nanotubes employed (reported above, see Experimental Section) were determined. Figure 1b shows a micrograph of the $PE_{83}M_6Al_{11}$ material prepared in a similar way. A thin coating of HDPE can be seen surrounding the CNT, confirming previous results on the same type of material.[20]

In order to observe the HDPE lamellar structure, samples were isothermally crystallized for 7 days at a rather high temperature (124 °C) to promote the formation of thick lamellae. Figure

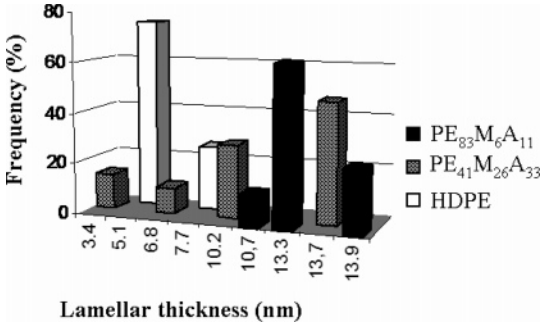

Figure 2. Lamellar thickness distributions after isothermal crystallization at 124 °C for 1 week.

1c,d shows the lamellar morphology surrounding the MWNT's in $PE_{83}M_6A_{11}$. The lamellae grow from the NT surface in a direction close to being perpendicular to the NT direction (even though a 90° angle was indeed found in some cases; in many other lamellar stacks this value was lower, as can be seen in some cases in Figure 1d). The lamellar morphology is almost like a bottle brush with the center being the CNT. This morphology indicates a strong nucleating effect of the CNT and resembles that of transcristalline growth around active nucleating fibers.[36] Since the chain direction is generally perpendicular to the lamellae, the general orientation of the chains is close to parallel (although some may form an angle) to the CNT axis. These results are generally in agreement with those found by Minus et al.[31] and Haggenmueller et al.,[32] who also reported crystal growth perpendicular to the CNT surface.

Figure 2 shows a histogram of lamellar thickness distribution obtained from micrographs like those shown in Figure 1c,d. Lamellar thickness in excess of 40 Å must have been produced during isothermal crystallization. A DSC heating scan performed to HDPE after isothermal crystallization exhibits bimodal melting (see Figure 3 and Table 2), with the higher temperature melting peak dominating over the low-temperature melting one. The higher melting peak (T_{m1}) corresponds to the fusion of the thicker isothermally crystallized lamellae, and the lower melting peak (T_{m2}) corresponds to the fusion of the thinner lamellae formed during cooling (after isothermal crystallization samples were quickly cooled to room temperature). In the case of the samples with CNT, the melting enthalpy of the higher melting peak was larger than in neat HDPE. In fact, in two of the samples in Figure 3, only the high-temperature melting peak was detected (see Table 2). It should also be noted that the peak melting point of the higher temperature melting peak was up to 5 °C higher (see Table 2) for the samples containing CNT than for neat HDPE, a remarkable change for a polyethylene sample.

Figure 2 is fully consistent with the DSC results of Figure 3 since, on the whole, thicker lamellae are observed for the samples with CNT than for neat HDPE. This is a novel and intriguing result since under isothermal crystallization conditions at the same undercooling the lamellar thickness produced should have been the same. Even considering the possible nucleation effect of CNT, the expectation would be a higher number of crystals, since nucleation is favored but of equivalent thermodynamic stability. The reason why the CNT are producing more stable crystals (as judged by their thickness) is unknown, but the experimental fact corroborated by both TEM and DSC is beyond any doubt, and it can be speculated that the way the polyethylene chains were grown on the surface of the CNT could be responsible for this effect. Furthermore, as we will see below, this trend is also consistent with results obtained by standard cooling from the melt and subsequent heating in the DSC, so it

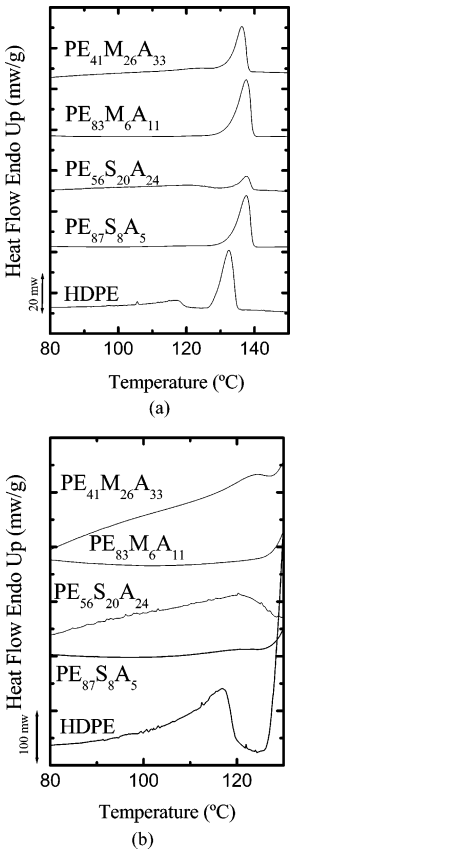

Figure 3. DSC heating scans after 1 week of isothermal crystallization of the samples at 124 °C (followed by quenching to room temperature). In (a) the full temperature range is presented, and in (b) a narrower temperature range with a higher magnification is shown, so that details of the first melting peak can be observed.

is not a characteristic of isothermal crystallization but it is also produced under dynamic conditions (see Table 3 and Figures 4 and 5). The reason behind this interesting behavior must be related to the way the polymer has been produced on the surface of the CNT by the in-situ polymerization filling technique.

3.2. Thermal Characterization. *3.2.1. Standard DSC Scans.* All samples were cooled from the melt (170 °C) to 0 °C while registering their DSC cooling scans at 10 °C/min, and then their subsequent heating scans were recorded at the same scanning rate. The DSC scans can be seen in Figure 4. All the samples exhibit a single crystallization exotherm and a corresponding single melting endotherm; the main changes are in the characteristic onset and peak crystallization and melting temperatures and in the values of the associated enthalpies in addition to peak broadening effects in the nanocomposites as compared to HDPE. The DSC scans have been normalized by dividing the heat flow axis by the weight of the HDPE content in the sample, so the areas under the exotherms and endotherms represent the changes in the HDPE crystallinities. Table 3 shows all the characteristic temperatures and enthalpy values extracted from Figure 4, while Figure 5a,b shows the changes in the most representative thermal properties as a function of CNT content. The melting points of the as-synthesized samples (i.e., first heating scans) are not presented since their values were very similar to those of the second heating scans presented in Table 3.

The crystallization temperatures increase with CNT content as a result of the nucleating action of the CNT. The nucleating action saturates at higher levels of CNT loading and even decreases in some cases. Conversely, the degree of crystallinity (Figure 5b) decreases monotonically as the amount of CNT

Table 2. Melting Temperatures and Enthalpies after Isothermal Crystallization for 1 week at 124 °C (from Figure 3)

	melting process 1			melting process 2		
composition	T_m^1 onset (°C)	T_m^1peak (°C)	ΔH_m^1 (J/g)	T_m^2 onset (°C)	T_m^2 peak (°C)	ΔH_m^2 (J/g)
HDPE	128.2	132.9	137.2	104.8	117.0	47.5
$PE_{87}S_8A_5$	132.3	137.6	123.7		122.0	
$PE_{33}S_{36}A_{31}$	134.2	137.7	10.4	107.1	120.2	8.4
$PE_{83}M_6A_{11}$	132.6	137.6	138.4			
$PE_{41}M_{26}A_{33}$	132.4	136.7	42.0	116.4	123.0	1.4

Table 3. Crystallization Temperatures, Melting Temperatures, and Enthalpies Extracted from Figure 4

composition	$T_{m,onset}$ (°C)	$T_{m,\ peak}$ (°C)	ΔH_m (J/g)	$T_{c,onset}$ (°C)	$T_{c\ ,peak}$ (°C)	ΔH_c (J/g)
HDPE	123.2	129.6	179.6	120.5	118.3	214.9
$PE_{87}S_8A_5$	124.3	133.3	127.1	123.5	120.3	145.7
$PE_{56}S_{20}A_{24}$	120.7	131.4	46.7	123.9	120.6	72.7
$PE_{33}S_{36}A_{31}$	114.3	129.5	15.5	124.5	119.1	41.3
$PE_{82}D_8A_{10}$	125.5	133.5	126.9	123.9	121.0	151.4
$PE_{60}D_{17}A_{23}$	122.0	131.9	69.8	124.7	121.5	88.9
$PE_{44}D_{26}A_{30}$	118.2	130.6	43.1	124.8	121.6	44.6
$PE_{83}M_6A_{11}$	126.2	133.6	139.6	123.0	120.2	139.4
$PE_{68}M_{11}A_{21}$	124.8	132.4	101.0	123.4	120.3	102.1
$PE_{41}M_{26}A_{33}$	120.4	130.1	51.1	123.9	119.4	50.0
$PE_{93}M_6A_1$[a]	123.3	129.8	179.8	120.7	117.8	162.7

[a] System mixed in the DSC pan with untreated CNT.

increases. This is an unexpected behavior when compared to the usual action of nucleating agents, since they normally do not affect crystallinity or tend to increase it; however, the amounts employed rarely exceed 3%. In this case, the drop in crystallinity is certainly more pronounced at higher concentrations. Given that CNT possess a remarkably high superficial area, at high contents they are probably interfering with crystal growth. It should be noted that when the CNT content increases, the amount of Al_2O_3 residues, which is a byproduct of the synthesis (see Experimental Section), also increases. Therefore, the PE phase can amount to just 50% or even 30% of the sample. At such high amounts of fillers (both CNT and Al_2O_3), the interference with the crystal growing process can be considerable. The highest effect on the crystallinity was found for the nanocomposites with SWNT, as expected since they will have the maximum surface area in contact with the HDPE as compared to DWNT and MWNT since they have the lowest diameter and highest aspect ratio.

Another interesting phenomenon shown in Figure 5a is the increase in T_m observed in samples with CNT as compared with neat HDPE. This increase in T_m is progressively reduced as the content of CNT increases. This effect, once more, is consistent with the morphological results obtained by isothermal crystallization that indicate an improved thermodynamic stability of the crystals formed under identical conditions as compared to neat HDPE. The effect seems to disappear for the highest CNT content, as a result of the same interference effect that is reducing the crystallinity of the samples. However, the effect of the CNT is still there if one compares neat HDPE and $PE_{36}S_{33}A_{31}$ (see Table 3 and Figure 5); the melting points are almost the same, but the crystallinity in the nanocomposite is only 15% as compared to 60% for neat HDPE. In spite of the fact that the PE crystal growth is affected by the large content of SWNT and aluminum oxide, it can still develop lamellar crystals that are as thick as those of HDPE under dynamic conditions.

One is tempted to explain the trends shown in Figure 5a on the basis of a simple nucleating agent action. However, HDPE is a polymer with an already high nuclei density; therefore, normally, even when it is nucleated by an external agent, its melting point should not be greatly affected. Also, the metastability of polymeric crystals is usually manifested in kinetic conditions such as those applied in Figure 4. A large change in peak T_c is normally required in order to obtain a small change in peak T_m; this is a valid statement even under isothermal conditions, and it is also the reasoning behind the extrapolation of Hoffman−Weeks to obtain the equilibrium melting point of polymers. If Table 3 is examined in detail, we can see that in some cases the increase in peak T_c obtained by incorporating CNT (as compared to the peak T_c temperature in HDPE) is

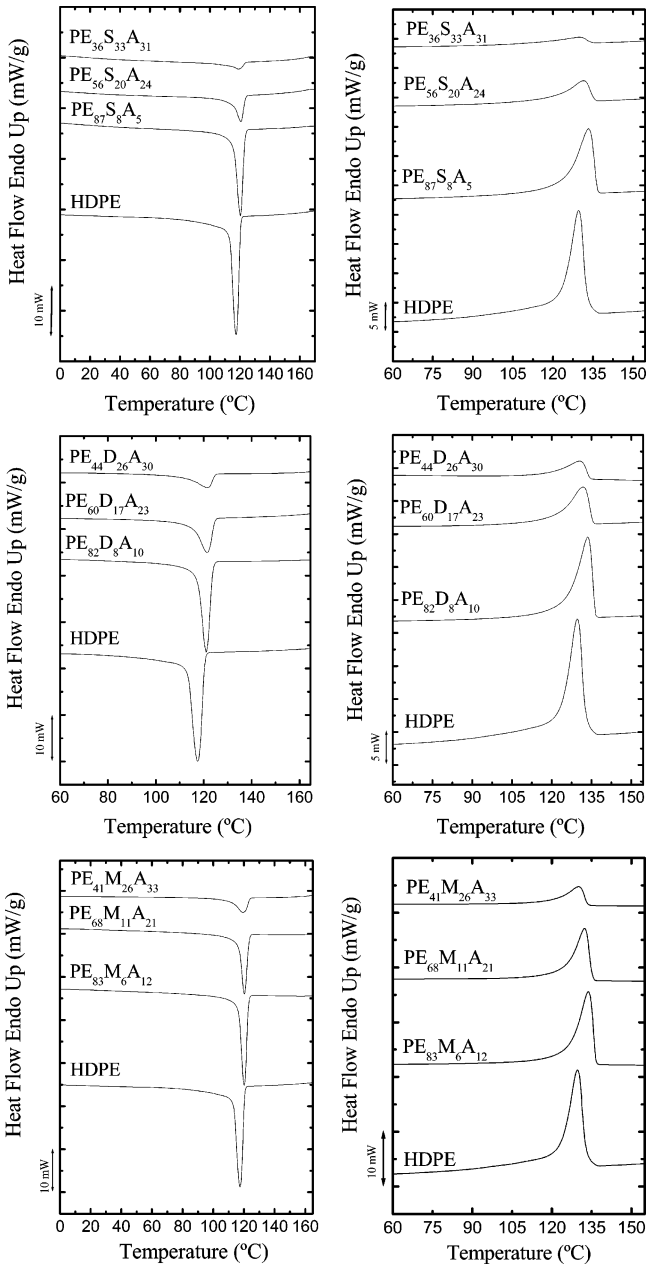

Figure 4. DSC cooling and heating scans for single-wall nanotube system ($PE_xS_yA_z$), double-wall nanotube system ($PE_xD_yA_z$), and multiwall nanotube system ($PE_xM_yA_z$). All scans were performed at 10 °C/min.

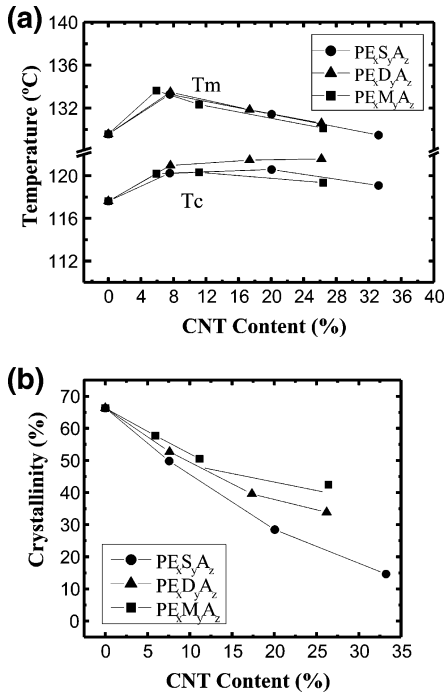

Figure 5. (a) Influence of CNT content on peak crystallization and melting temperature (T_c and T_m) for HDPE/CNT nanocomposites. (b) Influence of CNT content on the degree of crystallinity (X_c) for HDPE/CNT nanocomposites.

almost the same as that obtained in T_m. The change in T_m cannot therefore be due to the change in peak T_c; otherwise, we would be in the equilibrium case where a change in T_c is reflected in a change in T_m of the exact same magnitude. In any case, the increase in lamellar thickness with the presence of CNT was demonstrated in Figures 1−3 for isothermally crystallized samples, where dynamic effects are minimized.

With the purpose of establishing whether the changes encountered in the thermal properties are related to the way the nanocomposites were prepared, simple physical blends of HDPE and neat MWNT (untreated) were performed by mechanical melt mixing in a DSC capsule (employing a glass rod as a mixer). The results are also shown in Table 3, and they show that in this case the CNT are not influencing the thermal behavior of HDPE in spite of being present in 5.7%, the same proportion that caused the remarkable nucleating influence on the nanocomposites prepared by in-situ polymerization. Since the HDPE employed here was polymerized with exactly the same catalytic metallocene-based system used in the preparation of the in-situ nanocomposites, we believe the Al_2O_3 is not responsible for the remarkable nucleating action detected in the nanocomposites, since it is also present in the HDPE (see Table 1). Therefore, we must conclude that it is the way the nanocomposites were prepared what makes their thermal properties unique.

Other works have found that upon addition of CNT the crystallinity of the matrix polymer increases or does not vary. Minus et al.[31] found increases of up to 40% in crystallinity, as determined by WAXS, of poly(vinyl alcohol) (PVA) upon SWNT addition (these nanocomposites were prepared in solution). While Haggenmueller and co-workers[32] found no variation in the crystallinity of HDPE regardless of the amount of CNT added to this polymer (in a range from 1 to 30%). In this work, the CNT were added by a hot-coagulation method; therefore, the monomer was not polymerized as in the present case on the CNT surface.

3.2.2. Self-Nucleation Behavior. In view of the remarkable nucleating effect that CNT have on HDPE, we decided to study the self-nucleation behavior of all the nanocomposite samples in order to compare it with that of HDPE.

Figure 6 shows cooling scans from T_s and subsequent heating scans for HDPE in a T_s temperature range from 170 to 131.5 °C. No appreciable increases in crystallization temperature are observed upon decreasing T_s, a result that indicates a lack of domain II or self-nucleation domain. Such behavior, i.e., lack of domain II, was first encountered in highly confined crystallizable blocks within diblock and triblock copolymers.[37,38] This result shows that the neat HDPE employed here already possesses a very high density of heterogeneous nuclei, such that its own self-nuclei cannot apparently increase the overall nuclei density. The heterogeneous nuclei in HDPE usually stem from the synthesis; in this case the Al_2O_3 particles that remain in the polymer (after decomposition of metallocene aluminum oxide (MAO)) are surely the active nucleating species.

Close observation of the heating scans in Figure 6b indicates that a small high-temperature melting signal appears for a T_s of 131 °C (simultaneously, a small shift to higher temperatures of T_c peak was also obtained), which results from annealing of the unmolten crystals at T_s. This behavior is characteristic of domain III; this is a domain where annealing is observed besides self-nucleation. Hence, in this case the neat HDPE employed here does not exhibit domain II but a direct transition from domain I to domain III. The absence of domain II was also a characteristic of all the nanocomposites evaluated, and Figure 7 and Table 4 show the domain I−III transition temperatures for all the samples. In Figure 7, the transition from domain I to domain III is indicated with a vertical bar on top of the standard fusion endotherms of selected samples. It can be observed that the fraction of crystals that is needed for annealing to be detected (i.e., the fraction of crystals left unmolten at T_s, a value that is inversely proportional to the T_s value) is larger in the nanocomposites as compared to neat HDPE. The transition T_s temperatures from domain I to III are very similar for all the different types of nanocomposites prepared (S, D, or M) and tend to be slightly lower as the content of CNT increases.

The efficiency of the CNT as nucleating agents was assessed employing the method proposed by Fillon et al.,[39] based on the self-nucleation behavior of the materials containing the nucleating agent as compared to the neat material. The efficiency is calculated by the following equation:

$$NE = \frac{T_{c,NA} - T_{c,PE}}{T_{c,max} - T_{c,PE}} \times 100 \qquad (1)$$

where $T_{c,NA}$ is the peak crystallization temperature of the polymer with the nucleating agent, $T_{c,PE}$ is the peak crystallization temperature of neat HDPE (118.3 °C), and $T_{c,max}$ is the maximum crystallization temperature after HDPE has been self-nucleated and annealed (119.2 °C).

As can be appreciated in Table 5, the results indicate that the efficiency in all cases is higher than 100%, an expected result since the crystallization temperature of the samples with CNT was always higher than the crystallization temperature of HDPE. This result implies that CNT are being more efficient in nucleating HDPE than its own crystals, possibly because of the way the chains were grown on the surface of the CNT, creating a remarkable nucleation enhancement.

At industrial level, solidification times are crucial for optimizing production; hence, nucleating agents can increase the rate of production of plastic parts. With just 5% of CNT, the peak crystallization temperature of HDPE can be increased up to 4 °C; it is possible that even lower amounts can also produced a

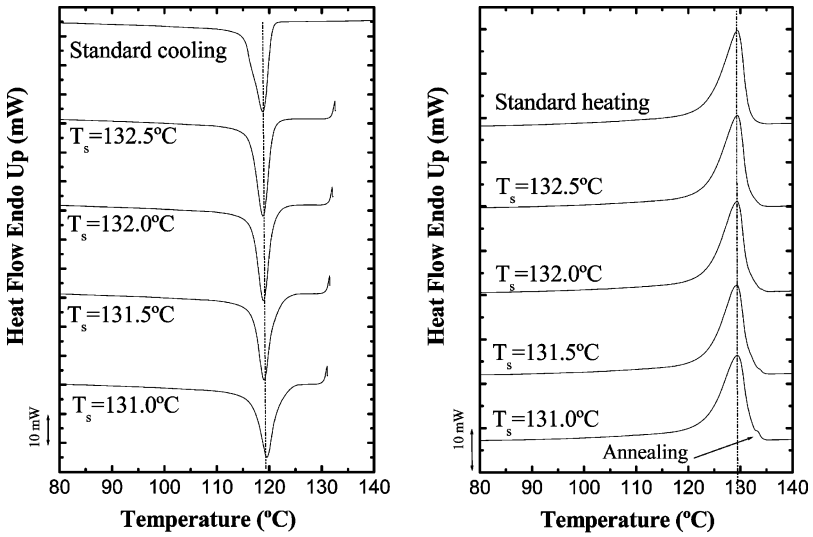

(a) (b)

Figure 6. Self-nucleation behavior of neat HDPE for selected self-nucleation temperatures (T_s): (a) DSC cooling scans from T_s and (b) DSC subsequent heating scans.

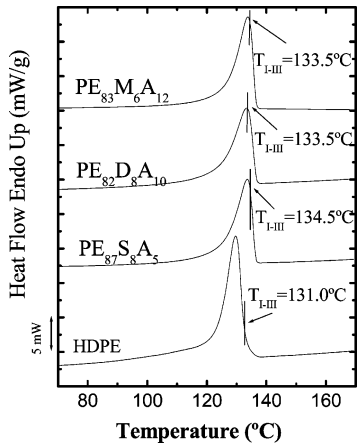

Figure 7. Standard DSC heating scans for selected samples showing the transition between domain I and domain III.

Table 4. Transitions between Domain I and Domain III for the Systems Evaluated

composition	T_{I-III} (°C)	composition	T_{I-III} (°C)
HDPE	131.0	$PE_{60}D_{17}A_{23}$	134.0
$PE_{87}S_8A5$	134.0	$PE_{44}D_{26}A_{30}$	133.0
$PE_{56}S_{20}A_{24}$	134.0	$PE_{83}M_6A_{11}$	134.0
$PE_{33}S_{36}A_{31}$	134.0	$PE_{68}M_{11}A_{21}$	134.5
$PE_{82}D_8A_{10}$	134.0	$PE_{41}M_{26}A_{33}$	132.0

Table 5. CNT Efficiency as Nucleating Agents for the Systems Evaluated

composition	efficiency (%)	composition	efficiency (%)
$PE_{87}S_8A_5$	259	$PE_{44}D_{26}A_{30}$	439
$PE_{56}S_{20}A_{24}$	317	$PE_{83}M_6A_{11}$	200
$PE_{33}S_{36}A_{31}$	199	$PE_{68}M_{11}A_{21}$	244
$PE_{82}D_8A_{10}$	298	$PE_{41}M_{26}A_{33}$	151
$PE_{60}D_{17}A_{23}$	440		

similar nucleating action. Besides, we have demonstrated that the PE chains polymerized on the surface of specially treated CNT prefer to nucleate around the CNT than on the very same HDPE crystals, and this also entails a specific bottle brush morphology which can also have a significant impact on the mechanical properties of the HDPE. The materials under study here can also be employed as a masterbatch of dispersible CNT. Therefore, mixtures of these materials with linear low-density polyethylene (which could have packaging applications) are being prepared, and the properties of such blends are being investigated.[40]

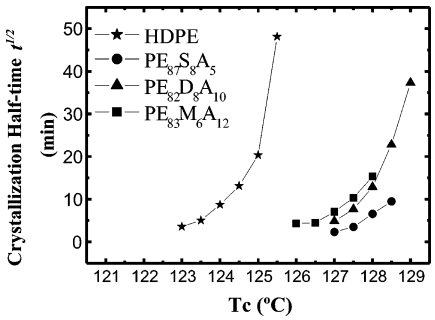

Figure 8. Overall crystallization half-time ($t_{1/2}$) for systems with lower contents of CNT.

3.2.3. Isothermal Crystallization. The isothermal crystallization of all samples was determined by DSC, and the results were fitted with the Avrami equation, a common tool to describe overall isothermal crystallization (including nucleation and growth). The Avrami equation can be expressed as[41,42]

$$1 - V_c(t) = \exp(-kt^n) \tag{2}$$

where V_c is relative transformation volume fraction at the crystallization time t, k is the overall crystallization rate constant which is a function of nucleation and growth, and n is the Avrami index. The Avrami index is a complex exponent whose value is related to the dimensionality of the growing crystals and to the time dependence of nucleation.[41,42] In order to fit the experimental data to the Avrami equation, we closely followed the procedure given in ref 42.

Figure 8 shows how the crystallization half-time (an experimental measure of the overall relative crystallization rate) depends on the crystallization temperature. It is evident that for all the in-situ-polymerized nanocomposite samples the supercooling needed for isothermal crystallization was much lower than for HDPE. The effect depends slightly on the CNT type, and it follows the order SWNT > DWNT > MWNT. This result is a direct consequence of the remarkable nucleation effect caused by the CNT, and at the same time it shows that if the

Table 6. Avrami Index (*n*) and Overall Crystallization Rate Constant (*k*) Obtained during Isothermal Crystallization for HDPE and Systems with Low Content of CNT

	HDPE		$PE_{87}S_8A_5$		$PE_{82}D_8A_{10}$		$PE_{83}M_6A_{11}$	
T_c (°C)	n	10^3K (min^{-n})	n	10^3K (min^{-n})	n	10^3K (min^{-n})	n	10^3K (min^{-n})
123.0	2.1	64.5						
123.5	2.1	33.0						
124.0	2.1	10.4						
124.5	2.0	4.99						
125.0	2.0	1.58						
125.5	2.2	0.23						
126.0							2.2	328
126.5							2.2	221
127.0			1.9	138	2.0	30.3	2.2	114
127.5			1.9	61.6	2.1	14.8	2.2	4.34
128.0			2.0	12.3	2.2	2.73	2.2	1.77
128.5			2.1	5.84	2.4	0.44		
129.0					2.4	0.12		

crystallization could be performed at the same T_c, the crystallization rate for the samples with CNT would be much faster. A similar result regarding the influence of CNT on the overall crystallization kinetics has already been reported in the literature for several crystallizable polymers such as PE,[32] iPP,[28,29] PVA,[43] PAN,[44] and thermoplastic elastomers (polyurethane).[45]

As stated above, the geometry of the CNT has a small influence on the crystallization kinetics, and as the diameter of the CNT is reduced, the crystallization rate is enhanced. A surface area effect, similar to that invoked when discussing Figure 5b, could also be responsible for this effect, since CNT surface area (at the same CNT content) should increase in the following order: SWNT > DWNT > MWNT.

Table 6 reports the values of *k* and *n*. The values of *k* closely followed the trend of the inverse crystallization half-time with crystallization temperature, as expected. On the other hand, the values of the Avrami index did not vary much and were always in the range 2.2−2.4. Since neat HDPE already had many active nuclei, the expectation would be an Avrami index of 3 if spherulitic superstructures were instantaneously formed. However, when the density of nuclei is so large, spherulites are very difficult to develop, since the nuclei are too close to each other to allow free 3D growth and the morphology resembles more 2D lamellar stacks that could explain the Avrami indexes close to 2 when instantaneous nucleation is in place. The bottle brush morphology observed in Figure 1 for the nanocomposites is also consistent with 2D lamellar staking and lack of well-developed 3D superstructures.

Haggenmueller et al.[32] reported reductions in Avrami indexes from 2 to 1.5 upon the inclusion of 1 wt % SWNT in a HDPE matrix. On the contrary, Grady et al.[28] found increases in the Avrami indexes from 2.2 to 2.8 when 0.6% CNT was added to the system. Therefore, no clear trend can be established so far.

3.3. Wide-Angle X-ray Diffraction (WAXS). Figure 9 shows WAXS diffractograms for neat HDPE and nanocomposites with the lowest concentrations of the three types of CNT. In all cases the crystalline structure of HDPE remains intact with the orthorhombic unit cell in the *Pnam* space group. The (110) and (200) reflections are located at 21.55° and 24.01° in 2θ, respectively. The (210) and (020) peaks are clearly distinguished. From Figure 9 it is clearly seen that there are no structural changes, and the crystallinity values are comparable for these low CNT concentrations. At higher CNT concentrations an important decrease in the crystallinity degree is observed (results not shown). The introduction of CNT in the semicrystalline polymer matrix in low amounts does not perturb either the 3D order of the lamellas or their perfection or their amount.

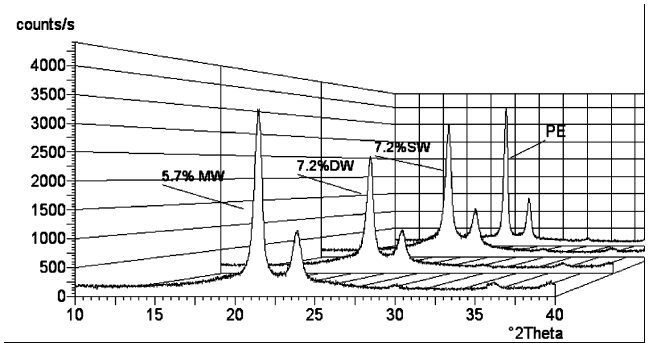

Figure 9. WAXS diffractograms for neat HDPE and selected in-situ HDPE/CNT nanocomposites.

4. Conclusions

An outstanding nucleating effect of CNT on the polyethylene matrix was found for the in-situ-prepared nanocomposites, regardless of the CNT type, in comparison to neat high-density polyethylene (HDPE) prepared under identical conditions but without CNT. The nucleating effect of the CNT was even more efficient than that produced by the HDPE own crystal fragments according to the self-nucleation studies, and therefore nucleating efficiencies higher than 100% were obtained. TEM and DSC results showed that under both isothermal and dynamic crystallization conditions the lamellae produced within the nanocomposite HDPE matrix are thicker than those produced in neat HDPE or in physical blends prepared by melt mixing of HDPE and untreated CNT. This remarkable lamellar stability was reflected in melting points up to 4 °C higher than neat HDPE. The in-situ-prepared nanocomposites crystallize much faster at equivalent supercoolings than neat HDPE because of the nucleating effect of CNT under isothermal conditions. The changes induced on HDPE by CNT are due to the way the nanocomposites were prepared; since the macromolecular chains grow from the surface of the nanotube where the metallocene-based catalyst has been deposited, this produces a remarkable nucleating effect and bottle brush morphology around the CNT. Wide-angle X-ray scattering studies demonstrated that the crystalline structure of the HDPE matrix within the in-situ-polymerized HDPE/CNT nanocomposites was identical to that of neat HDPE and did not change during isothermal crystallization.

Acknowledgment. The USB team acknowledges financial support from the Decanato de Investigación y Desarrollo of Simón Bolívar University through Grants GID-G02 and GID-G15. CIRMAP thanks Nanocyl S.A. (Sambreville, Belgium) for kindly providing the carbon nanotubes. This work was financially supported by "Région Wallonne" and European Community (FEDER, FSE) within the framework of ''Objectif 1: Materia Nova". CIRMAP thanks the "Belgian Federal Government Office Policy of Science (SSTC)" for general support in the frame of the PAI-5/03. S.B. thanks "European Community" for financial support in the frame of the Nanohybrid project (STREP NMP3-CT-2005-516972).

References and Notes

(1) Iijima, S. *Nature (London)* **1991**, *354*, 56.
(2) Ajayan, P. In *Handbook of Nanostructured Materials and Nanotechnology*; Nalwa, H. S., Ed.; Academic Press: New York, 2000; Vol. 5, p 575.
(3) Wang, C.; Guo, Z.; Fu, S.; Wu, W.; Zhu, D. *Prog. Polym. Sci.* **2004**, *29*, 1079.
(4) Ajayan, P.; Zhou, O. Z. *Top. Appl. Phys.* **2001**, *80*, 391.

(5) Ajayan, P. M.; Stephan, O.; Colliex, C.; Trauth, D. *Science* **1994**, *265*, 1212.
(6) Moniruzzaman, M.; Winey, K. I. *Macromolecules* **2006**, *39*, 5194.
(7) Velasco, C.; Martinez, A. L.; Lozada, M.; Alvarez, M.; Castaño, V. M. *Nanotechnology* **2002**, *13*, 495.
(8) Budert, H.; Haiber, S.; Brandl, W.; Marginean, G.; Heintze, M.; Bruser, V. *Diamond Relat. Mater.* **2003**, *12*, 811.
(9) Gojny, H.; Nastalczyk, J.; Roslaniec, Z.; Schulte, K. *Chem. Phys. Lett.* **2003**, *370*, 820.
(10) Gong, X.; Liu, J.; Baskaran, S.; Voise, R.; Young, J.; James, S. *Chem. Mater.* **2000**, *12*, 1049.
(11) Islam, M. F.; Rojas, E.; Bergey, D. M.; Jonson, A. T.; Yodh, A. G. *Nano Lett.* **2003**, *3*, 269.
(12) Moore, V. C.; Strano, M. S.; Haroz, E. H.; Hauge, R. H.; Smalley, R. E.; Schmidt, J.; Talmon, Y. *Nano Lett.* **2003**, *3*, 1379.
(13) Sabba, Y.; Thomas, E. L. *Macromolecules* **2004**, *37*, 4815.
(14) Regev, O.; Elkati, P. N. B.; Loos, J.; Koning, C. E. *Adv. Mater.* **2004**, *16*, 248.
(15) Park, C.; Ounaies, Z.; Watson, K. A.; Crooks, R. E.; Smith, J.; Lowther, S. E.; Conell, J. W.; Siochi, E. J.; Harrison, J.; St. Clair, T. L. *Chem. Phys. Lett.* **2002**, *364*, 303.
(16) Fia, Z.; Wang, Z.; Leanz, J. *Mater. Sci. Eng.* **1999**, *271*, 395.
(17) Zhang, X.; Liu, T.; Sreekumar, T. V.; Kumar, S.; Moore, V. C.; Hauge, R. H.; Smalley, R. E. *Nano Lett.* **2003**, *3*, 1285.
(18) Huang, X.; Brittain, W. J. *Macromolecules* **2001**, *34*, 3255.
(19) Zhang, Q.; Lippits, D. R.; Rastogi, S. *Macromolecules* **2006**, *39*, 658.
(20) Bonduel, D.; Mainil, M.; Alexandre, M.; Monteverde, F.; Dubois, P. *Chem. Commun.* **2005**, *6*, 781. Bonduel, D.; Bredeau, S.; Alexandre, M.; Monteverde, F.; Dubois, Ph. *J. Mater. Chem.* **2007**, *17*, 2359.
(21) Enikolopian, N. S. USSR Patent 763 379, 1976.
(22) Howard, E. G. US Patent, 4 097 447, 1978.
(23) Kaminsky, W.; Zielonka, H. *Polym. Adv. Technol.* **1993**, *4*, 415.
(24) Alexandre, M.; Martin, E.; Dubois, P.; Garcia-Marti, M.; Jérome, R. *Macromol. Rapid Commun.* **2000**, *21*, 931.
(25) Alexandre, M.; Beyer, G.; Henrist, C.; Cloots, R.; Rulmont, A.; Jerome, R.; Dubois, P. *Macromol. Rapid Commun.* **2001**, *22*, 643.
(26) Alexandre, M.; Pluta, M.; Dubois, P.; Jérome, R. *Macromol. Chem. Phys.* **2001**, *202*, 2239.
(27) Bhattacharyya, A. R.; Sreekumar, T. V.; Liu, T.; Kumar, S.; Ericson, L. M.; Hauge, R. H.; Smalley, R. E. *Polymer* **2003**, *44*, 2373.
(28) Grady, B. P.; Pompeo, F.; Shambaugh, R. L.; Resasco, D. E. *J. Phys. Chem. B* **2002**, *106*, 5852.
(29) Assouline, E.; Lustiger, A.; Barber, A. H.; Cooper, C. A.; Klein, E.; Wachtel, E.; Wagner, H. D. *J. Polym. Sci., Part B: Polym. Phys.* **2003**, *41*, 520.
(30) Probst, O.; Moore, E. M.; Resasco, D. E.; Grady, B. P. *Polymer* **2004**, *45*, 4437.
(31) Minus, M. L.; Chae, H. G. Kumar, S. *Polymer* **2006**, *47*, 3705.
(32) Haggenmueller, R.; Fischer, J. E.; Winey, K. I. *Macromolecules* **2006**, *39*, 2964.
(33) Fillon, B.; Wittmann, J. C.; Lotz, B.; Thierry, A. *J. Polym. Sci., Part B* **1993**, *31*, 1383.
(34) Lorenzo, A. T.; Arnal, M. L.; Sánchez, J. J.; Müller, A. J. *J. Polym. Sci., Part B* **2006**, *44*, 1738.
(35) Müller, A. J.; Arnal, M. L. *Prog. Polym. Sci.* **2005**, *30*, 559.
(36) Bassett, D. C. *Principles of Polymer Morphology*; Cambridge University Press: Cambridge, UK, 1991.
(37) Balsamo, V.; Paolini, Y.; Ronca, G.; Müller, A. J. *Macromol. Chem. Phys.* **2000**, *201*, 2711.
(38) Müller, A. J.; Balsamo, V.; Arnal, M. L. *Adv. Polym. Sci.* **2005**, *190*, 1.
(39) Fillon, B.; Lotz, B.; Thierry, A.; Wittmann, J. C. *J. Polym. Sci., Part B* **1993**, *31*, 1395.
(40) Trujillo, M.; Sánchez, J. J.; Müller, A. J.; Dubois, Ph. To be published.
(41) Mandelkern, L. In *Physical Properties of Polymers*, 3rd ed.; Mark, J. E., Ed.; Cambridge University Press: Cambridge, UK, 2004.
(42) Lorenzo, A. T.; Arnal, M. L.; Albuerne, J.; Müller, A. J. *Polym. Test.* **2007**, *26*, 222.
(43) Shaffer, M.; Windle, A. H. *Adv. Mater.* **1999**, *11*, 937.
(44) Ko, F.; Gogostsi, Y.; Ali. A.; Naguib, N.; Ye, H.; Yang, G. L.; Li, C.; Willis, P. *Adv. Mater.* **2003**, *15*, 1161.
(45) Koerner, H.; Price, G.; Pearce, N.; Alexander, M.; Vaia, R. *Nat. Mater.* **2004**, *3*, 115.

MA071025M